FEBS Letters

FEBS PRESS science publishing by scientists

EDITOR'S CHOICE

Axonemal doublet microtubules can split into two complete singlets in human sperm flagellum tips

Davide Zabeo, Jacob T. Croft and Johanna L. Höög

Department of Chemistry and Molecular Biology, University of Gothenburg, Gothenburg, Sweden

Correspondence
J. L. Höög, Department of Chemistry and Molecular Biology, University of Gothenburg, Medicinaregatan 9E, 41390 Gothenburg, Sweden
Tel: +46 31 786 3937
E-mail: johanna.hoog@gu.se

(Received 27 February 2019, revised 29 March 2019, accepted 3 April 2019, available online 19 April 2019)

doi:10.1002/1873-3468.13379

Edited by John Briggs

Motile flagella are crucial for human fertility and embryonic development. The distal tip of the flagellum is where growth and intra-flagellar transport are coordinated. In most model organisms, but not all, the distal tip includes a 'singlet region', where axonemal doublet microtubules (dMT) terminate and only complete A-tubules extend as singlet microtubules (sMT) to the tip. How a human flagellar tip is structured is unknown. Here, the flagellar tip structure of human spermatozoa was investigated by cryo-electron tomography, revealing the formation of a complete sMT from both the A-tubule and B-tubule of dMTs. This different tip arrangement in human spermatozoa shows the need to investigate human flagella directly in order to understand their role in health and disease.

Keywords: axoneme; cilia; cryo-electron microscopy; cryo-electron tomography; fibrous sheath; singlet region

Flagella, also called cilia, are cellular organelles that can be found in most organs in the human body as well as in many other multicellular and unicellular eukaryotes. They are membrane-covered cellular extensions that can act as a source of motility [1–5], a sensory organelle [6–8] and often a combination of both [9–11]. Ciliopathies are a group of genetic diseases caused by malfunctions of human flagella and when such diseases specifically affect motile flagella they are called primary ciliary dyskinesia (PCD). PCD heavily affects patients' health with recurring pulmonary infections, deafness and infertility amongst many other medical issues [12–16].

The flagellar proximal end emanates from a cytoplasmic basal body, which contains a ring of nine triplet microtubules (MTs) [17–20]. Each triplet contains a complete 13-protofilament A-tubule as well as incomplete 10-protofilament B- and C-tubules. The 13-protofilament symmetry is set by the γ-tubulin ring complex in the basal body [21–23]. In the transition zone, at the protrusion point from the cell, the C-tubules end while the A- and B-tubules keep extending as a doublet MT (dMT) [24]. In motile flagella, two MTs called the central pair (CP) start in the transition zone and extend alongside the dMTs, creating an ordered 9 + 2 MT arrangement. Together with the radial spokes, which connect the CP to the dMTs [25], and other associated protein complexes, this arrangement is called an axoneme (Fig. 1A), which is the molecular machine that generates the motility of flagella. The structure of the axoneme is considered to be conserved throughout evolution [1,4,26,27].

However, a structural variability among flagella of different species is becoming increasingly apparent [15,28–30]. Therefore, the information gained from model organisms may not directly apply to human flagella. Since ultrastructural information from human flagella is limited, in this study cryo-electron tomography (cryo-ET) was performed on intact human sperm tails.

Abbreviations

CP, central pair; dMT, doublet microtubule; EM, electron microscopy; ET, electron tomography; MT, microtubule; PCD, primary ciliary dyskinesia; PM, plasma membrane; sMT, singlet microtubule.

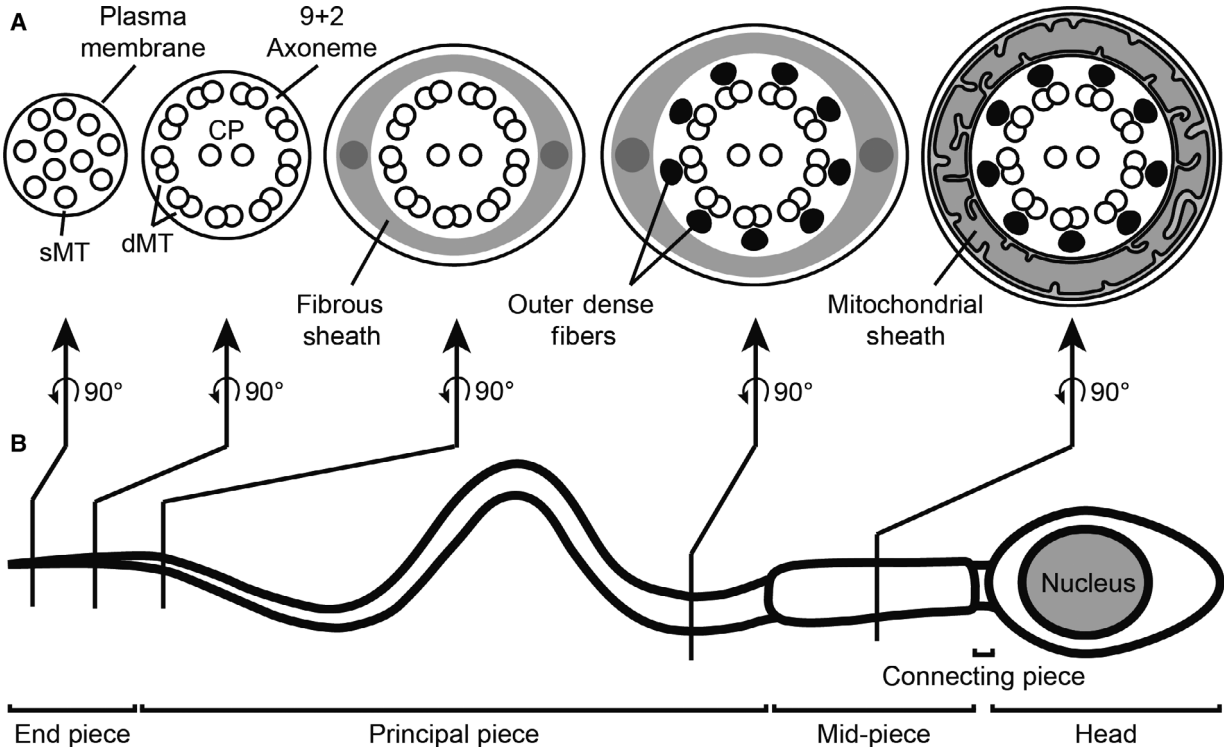

Fig. 1. Ultrastructure of mammalian spermatozoa. (A) Cartoon cross sections through the sperm flagellum illustrate its internal ultrastructure. The sperm tail distal tip contains spatially disorganized sMTs. More proximally, MTs are organized in an axoneme with nine dMTs and two CP MTs (9 + 2 arrangement). Even more proximal parts of the sperm tail are surrounded and protected by the FS [31,38] and by the outer dense fibers, that enhance structural integrity [34,35] and modulate the flagellar beat [36,37]. The mitochondrial sheath that wraps around the tail's mid-piece provides energy for cell motility. The arrows indicate which flagellar regions the cross sections represent. (B) The flagellum is divided into three structural regions. The most distal segment of the sperm flagellum is the end piece, which is defined by the absence of the FS. The principal piece includes most of the tail length and is protected by the FS. The mid-piece is defined by the presence of the mitochondrial sheath wrapped around it. The connecting piece (also called neck) links the spermatozoon head to its flagellum. The head is the most anterior part of the cell and it carries the genetic material in the nucleus.

In our model of choice, the mammalian spermatozoon, the flagellum is divided into three pieces (Fig. 1B) [31]. Starting at the distal tip, the end piece, the flagellum simply consists of the axoneme and the plasma membrane (PM) around it, without any supplementary structures. In the distal segment of the end piece, called the singlet region, the axonemal 9 + 2 symmetry is lost and the MTs extend as singlets [13,32,33]. In the principal piece, which includes most of the flagellum length, the axonemal dMTs are supported by nine outer dense fibers, which are thought to protect the flagellum integrity [34], to stabilize the axonemal structure [35] and to modulate the power and propagation of its beat [36,37]. In addition, the axoneme and outer dense fibers in the principal piece are surrounded and protected by the fibrous sheath (FS), a protein matrix with a rib-like structure [31,38]. In the mid-piece, a mitochondrial sheath wraps around the axoneme and outer dense fibers, providing energy for the motility of the cell [31].

The most distal tip is where the flagellum can grow and shrink. Therefore, it functions as a molecular traffic hub, where all the materials required to build the flagellum are delivered *via* the intra-flagellar transport system [39]. There is an ultrastructural heterogeneity between the distal tips of different organisms [28,30]. In the flagellar tips of model organisms like *Chlamydomonas reinhardtii* or *Tetrahymena thermophila*, the incomplete B-tubules of dMTs end and the A-tubules extend together with the CP to the tip extremity, creating the singlet region [40–42]. However, this region is completely absent in other models like *Leishmania mexicana* and *Trypanosoma brucei* [30,43,44]. In rodent spermatozoa, the singlet region includes the CP together with pairs of 'duplex' MTs – singlet MTs (sMT) extensions of A- and B-tubules from the same dMT [32]. In neuronal cilia of the nematode *Caenorhabditis elegans,* polyglutamylation of α-tubulin TBA-6 induces dMTs to split into complete A- and B-tubules, affecting ciliary ultrastructure and function [45–47]. In

this system, B-tubules elongate as complete sMTs but reconnect with their corresponding A-tubules before terminating [45,46].

The human singlet region contains up to 18 different sMTs [13,33,37]. Since there are only nine A-tubules and two CPs, any tip containing more than 11 sMTs suggests that the B-tubules in the 9 + 2 axoneme might be able to extend as complete sMTs as well. Our working hypothesis is therefore that the B-tubule can extend as a sMT in human sperm tails. To test this hypothesis, we examined the structure of the flagellar tips and the singlet region in human spermatozoa using cryo-ET. These singlet regions revealed high variation in MT number and termination pattern between cells. Splitting of dMTs into two sMTs was directly observed, confirming our hypothesis that incomplete B-tubules can extend as complete sMTs in human flagella. Alternatives to the γ-tubulin template model to establish the conventional 13-fold symmetry of MTs have been described *in vitro* [48,49] and our results suggest that such alternative models may function *in vivo* as well. This study is the first to describe the 3D architecture of the human flagellar tip by ET, and the results highlight the diversity of flagellar structures across evolution.

Materials and methods

Sample collection and plunge freezing

Human sperm was donated by three healthy men and plunge-frozen within 1–3 h from ejaculation time. Bull sperm was collected by VikingGenetics (Skara, Sweden), diluted in OptiXcell medium (IMV Technologies, L'Aigle, France), stored at 4 °C upon arrival to the laboratory and frozen for electron microscopy (EM) within 4 days from collection. A Vitrobot climate-controlled plunge freezer (FEI, Eindhoven, Netherlands) was used for plunge freezing of human and bull sperm. Prior to plunge freezing, 1 μL of gold fiducials was mixed in 4 μL of ejaculate and the 5 μL mix was blotted for 3 s (human) or 5 s (bovine). Leftover cells were examined under the light microscope, where their motility ensured that viable spermatozoa had been frozen.

High-pressure freezing and freeze substitution

Bovine spermatozoa were prepared using high-pressure freezing followed by freeze substitution. Undiluted bull ejaculate was mixed with an equal amount of 1× PBS and then concentrated by centrifugation at 300 ***g*** for 30 s. The supernatant was removed and cells were washed with 1× PBS and concentrated again. Concentrated cells were loaded onto aluminum carriers and high-pressure frozen in a Wohlwend Compact 3 (M. Wohlwend GmbH, Sennwald, Switzerland). Freeze substitution in acetone with 2% UA was initiated at −90 °C and the temperature was increased 3 °C per hour to −50 °C. Thereafter the cells were infiltrated and embedded in lowicryl HM20 resin polymerized by UV light. 50 nm thin sections were prepared and placed on formvar-coated copper slot grids. Sections were stained with 2% uranyl acetate and Reynold's lead citrate [50].

Data acquisition

Cryo-EM/ET of human sperm was done as described previously [33]. Cryo-EM on bull sperm was performed on a Titan Krios operated at 300 kV with a Falcon3 detector (FEI). Room temperature EM of bull spermatozoa thin sections was performed on a Tecnai T12 operated at 120 kV with a Ceta CMOS 16M camera (FEI).

Data analysis

Montages of all imaged cells were reconstructed by aligning overlapping cryo-electron micrographs. For the 23 cells whose tip was visible, the flagellum thickness was measured with IMOD [51] as the distance between the PM on each side of the flagellum. Three cells (out of 23) were excluded from the analysis because of large deformations of the flagellar membrane (Fig. S4). Data points were chosen every 100 nm up to 5 μm away from the tip and every 1 μm up to 29 μm away from the tip. Thickness values of 18–20 sperm tails were included for each data point of the end piece and 5–18 tails were included for each data point of the principal piece, depending on what extent of the sperm tail could be imaged (Fig. 2F). The distance between the flagellum tip and the end of the FS could be measured in 19 cells. The average value was used to define the end piece length.

All cryo-electron tomograms were calculated and CTF-corrected with eTomo [51]. sMTs and dMTs were independently counted in each tomogram (Fig. S1) and the extent of the singlet region was defined as the distance between the tip and the point where the number of sMTs equals that of dMTs. Due to the long singlet region of human spermatozoa, it is impossible to trace MTs back enough to distinguish between CP and extensions from dMTs, therefore in this work all MTs in the singlet region are collectively called sMTs. Sub-tomogram averaging of the dMT splitting events (Video S2) was performed with PEET [3].

Results

Variability in flagellar thickness correlates to microtubule number and presence of fibrous sheath

In order to investigate the ultrastructure of human flagella, cryo-electron tomograms were acquired on the

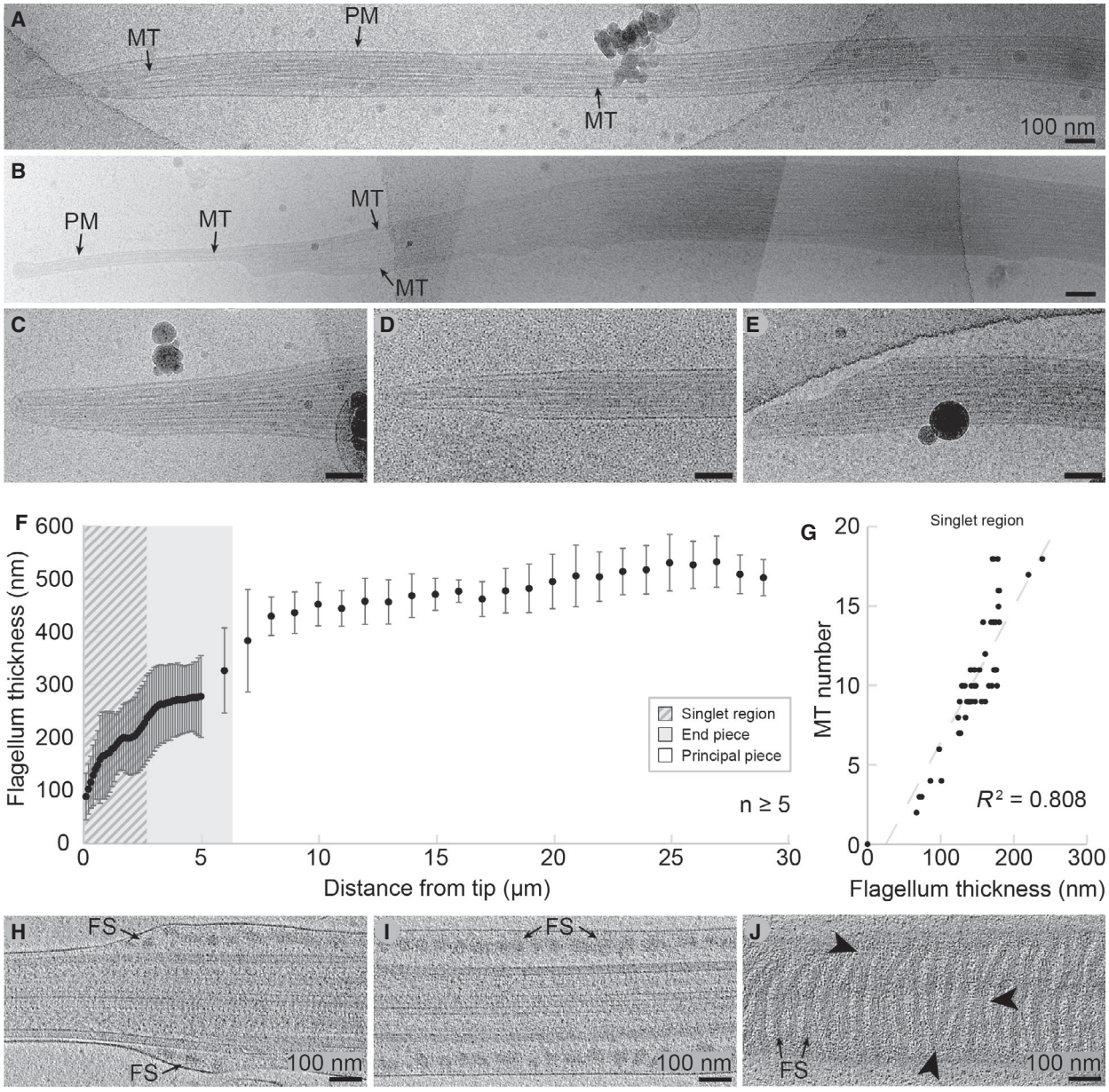

Fig. 2. The human sperm tail thickness correlates to the MT number in the end piece and to the presence of FS in the principal piece. (A–E) Montaged or single frame cryo-EM of human spermatozoon end pieces highlight morphological heterogeneity in sperm tails. The PM and the MTs of the flagellum are clearly visible. (F) The thickness of the flagellum increases with the distance from the tip. The striped background indicates the measured average extent of the singlet region and the gray background indicates the measured average extent of the end piece. Each data point represents the mean thickness of at least five individual flagella measured from montages of cryo-EMs (up to 20 flagella per data point in the end piece). The high standard deviation (error bars) is due to the intrinsic heterogeneity of the samples. (G) Cryo-ET revealed that the MT number correlates with the flagellum thickness in the singlet region (R^2 = 0.808). dMTs were counted as two MTs. (H–J) 23 nm-thick tomographic slices through the principal pieces of three different human sperm cells. (H) Transition point between the end piece and the principal piece. Longitudinal (H–I) and tangential (J) views of the principal piece reveal the rib-like morphology of the FS. Arrowheads indicate interconnections between adjacent ribs. All scale bars are 100 nm.

end pieces of 23 spermatozoa. Additionally, 2D montages of cryo-electron micrographs of the sperm tail were acquired for each imaged cell, so that the position of each tomogram could be measured. A great morphological variability between different cells was observed in the montages (Fig. 2A–E). Some end

pieces had a constant thickness before gradually tapering to a round tip (Fig. 2A), another sperm tip ended with only one sMT at the extremity (Fig. 2B). Individual sperm cells also showed large variability in flagellum thickness. The thickness was measured at regular intervals from the tip in cryo-EM montages (Fig. 2F and Video S1).

The largest change in thickness was observed within the most distal 8 μm, where the flagellum went from a tip thickness of 89 ± 44 nm (mean ± SD) to 429 ± 36 nm (Fig. 2F). In particular, the thickness mostly varied in two flagellar regions: at the distal 3 μm of the tip, including the singlet region, and approximately between 5 and 8 μm from the tip, corresponding to the transition between the end piece and the principal piece (Fig. 2F). Within the principal piece, the flagellar thickness only slightly but significantly varied, reaching 501 ± 34 nm at 29 μm from the tip (*t*-test between 8 and 29 μm from tip, $P < 0.002$). All data points had high standard deviation values, which reflects the observed high degree of heterogeneity between individual cells.

In this study, the singlet region was defined as the distance between the tip and the point where singlet and dMTs are present in equal number. Singlet and dMTs were counted for each acquired tomogram (Fig. S1) and the singlet region length was measured in three cells (2.35, 2.4 and 3.2 μm, respectively), averaging to 2.7 μm. In the singlet region, no large structures other than MTs nor connections between MTs were seen. In addition, the axonemal symmetry was disrupted and the radial spokes were absent. The flagellum thickness positively correlated with the MT number ($R^2 = 0.808$, Fig. 2G), suggesting that the MTs may be the main factor determining flagellum thickness at the tip. The MT number found in the singlet region was greatly variable, ranging from 2 to 14 sMTs, and no dMTs were ever observed closer than 1.6 μm to the tip (Fig. S1). In addition, the CP was found to terminate before other MTs in tomograms of two individual cells.

The end piece length was measured as the distance between the tip and the starting point of the FS, corresponding to an average of 6.3 μm ($n = 19$). Analysis of the tomograms revealed that the increase in thickness observed at the transition point into the end piece is caused by the start of the FS, whose structure was included in 11 tomograms at different distances from the tip (Fig. 2H–J). The FS started close to the axoneme but without any apparent auxiliary structure (Fig. 2H). It then enveloped the entire principal piece with its filamentous and interconnected rib-like structure, which was visible in longitudinal (Fig. 2I) as well as in tangential view (Fig. 2J).

In summary, these results indicate that the number of MTs may be the main factor in determining flagellar thickness in the end piece and that auxiliary structures like the FS are responsible for spermatozoa thickness in the principal piece.

Doublet microtubules can split into two singlet microtubules in human sperm flagella

Three sperm tail tips were included among the acquired tomograms (Fig. S2). In order to gain more insight into the ultrastructure of the singlet region, their MT number was counted at regular intervals from the tip, revealing diverse MT termination patterns (Fig. 3A). MTs could terminate as far away from the flagellar tip as 1 μm, some extended all the way to the tip and most MTs ended approximately 300–400 nm away from it. The MT number varied between the three tips, which, respectively, contained 10, 11, and 14 sMTs (Fig. 3A). The third flagellar tip, shown in cross-view (Fig. 3B–C), stood out for having 14 complete MTs, which is more than the 11 MTs the nine A-tubules and two CP MTs would form together. This observation supports the hypothesis that dMTs can generate two sMTs in human flagellum end pieces.

In an attempt to understand which axonemal MTs the sMTs extend from, tomograms of human spermatozoa that were acquired between 1 and 3.5 μm away from the tip were examined. A tomogram acquired 2 μm from the tip revealed dMTs transitioning into the singlet region by three different modes (Figs 3D–F, S3 and Video S2). As hypothesized, A-tubules and B-tubules originating from the same dMT split apart and continued as two complete sMTs ($n = 3$; Figs 3D and S3A–C). In other instances, the B-tubule simply terminated while the A-tubule extended ($n = 2$; Figs 3E and S3D–E). Finally, on one occasion, the B-tubule split apart from the A-tubule and kept extending as an incomplete and open MT (Figs 3F and S3F). Tomograms of two other cells also included the transition of the complete axoneme into the singlet region, however, they did not contain more than 11 sMTs. In these tomograms, all B-tubules terminated while the A-tubules extended to the tip, once again revealing a structural variability in the human sperm tip.

All 14 MTs in the end piece shown in Fig. 3B–C were successfully used for sub-tomogram averaging in a previous study [33], confirming that they were all complete 13-protofilament MTs. Therefore, the *de novo* formation of three protofilaments had somehow initiated on the incomplete 10-protofilament B-tubules. In addition, while the recently discovered

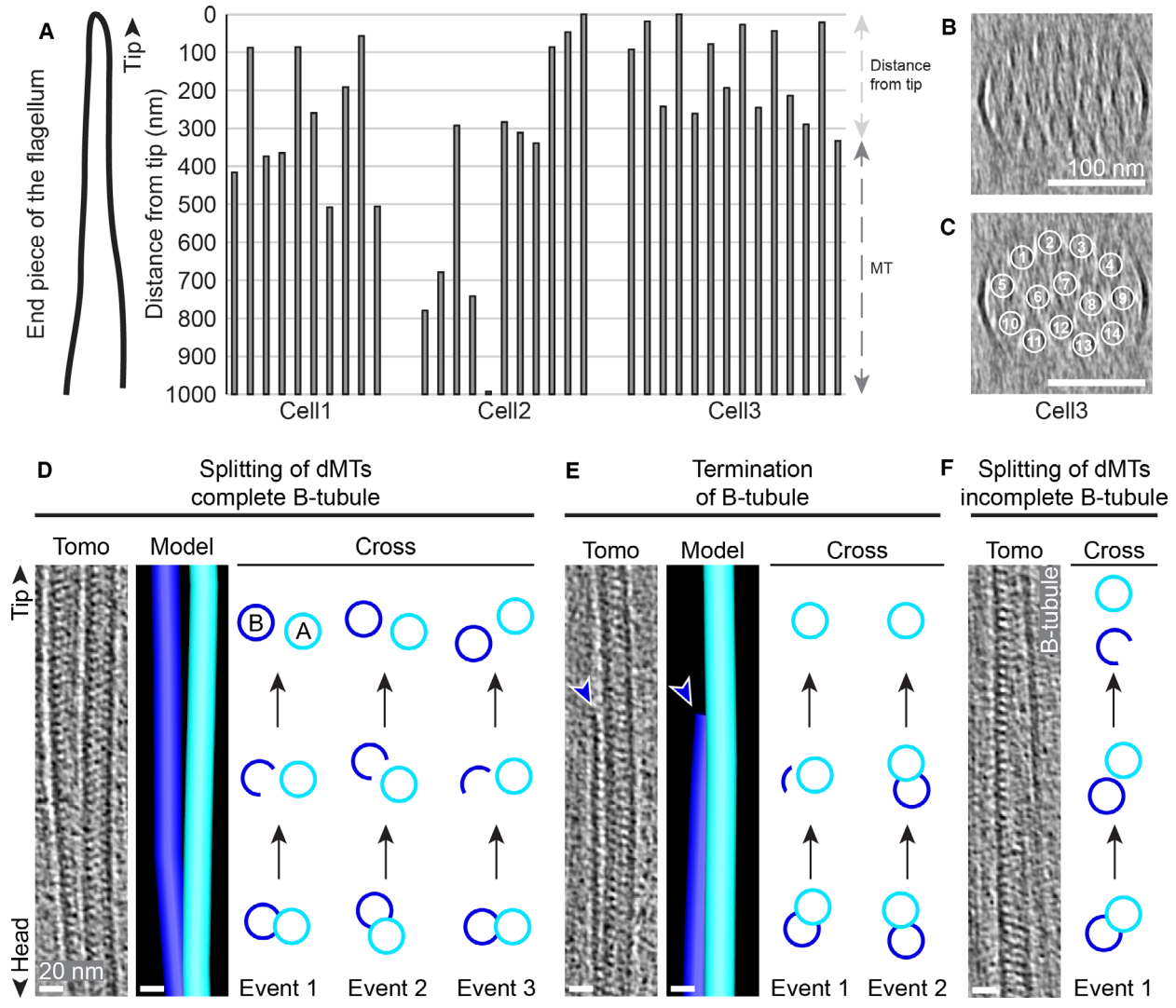

Fig. 3. dMTs can split into two complete sMTs in human flagella. (A) The distance between the MT termination point and the flagellum tip was measured in cryo-ETs for each MT in the singlet region of three different sperm cells. Tomographic views of the three imaged tips are shown in Fig. S2. The tips contained 10, 11, and 14 sMTs, respectively. The vertical bars represent sMTs (in random order), the top of the graph represents the flagellum tip and the spacing between them represents the distance of the MT termination points from the tip. (B–C) 23 nm-thick tomographic cross-sectional slices of the singlet region in cell3 from panel A, containing 14 sMTs. The two panels show the same image, but sMTs are circled and counted in panel C. (D–F) dMTs can transition into singlets by three modes. (1) The A- and B-tubules split into two complete sMT (D); (2) The B-tubule terminates while the A-tubule continues into the singlet region (E); (3) The B-tubule splits from the A-tubule and continues into the singlet region as an incomplete MT (F). A-tubules are drawn and marked in light blue and B-tubules in dark blue. Panels show one example for each transition mode in longitudinal tomographic views (Tomo) and models. Cross-view MT models (Cross) are shown for each observed event. Black arrows connect different cross-view models of the same dMT from most proximal to most distal. Dark blue arrowheads point at the B-tubule termination point. Panel F does not contain a longitudinal model and includes a tomographic view of the incomplete extension of the B-tubule. Additional tomographic views of each transition mode are shown in Fig. S3. Longitudinal views are 8 nm-thick tomographic slices. Scale bars are 100 nm in panels B–C and 20 nm in panels D–F.

TAILS structure [33] was decorating the lumen of every MT in the tomogram with splitting dMTs, no obvious electron density was observed to specifically localize at the splitting points. We conclude that in human flagellar end pieces, the B-tubule can sometimes, but not always, extend as a separate sMT.

Doublet microtubules can also split into two singlet microtubules in bovine sperm flagella

Bovine sperm flagella were analyzed to determine whether splitting of dMTs occurs in other mammalian sperm tips as well. Electron microscopy of thin

sections of high-pressure frozen bull ejaculate confirmed the presence of 18 and 15 sMTs in two different singlet regions, respectively (Fig. 4A–D). In addition, cryo-EM of the flattened tip of a bovine spermatozoon allowed direct visualization of dMT splitting and B-tubule termination, as observed in human flagella (Fig. 4E). The analyzed tip contained at least 16 sMTs, five distinct dMT splitting events and one B-tubule termination event. Therefore, different modes of dMT transition into the singlet region, including extension of a B-tubule singlet, are conserved in both bovine and human spermatozoa.

Discussion

This study presents the first cryo-ET analysis of the cellular structure of intact human flagella, in particular human sperm tails. 3D reconstructions of close to natively preserved sperm cells revealed that their distal tips are greatly heterogeneous and not directly comparable to model organisms such as *C. reinhardtii* or *T. brucei*. For instance, in human spermatozoa, the CP can terminate before any other axonemal MT (Fig. S1), unlike in *C. reinhardtii* [41,42], and a long singlet region is present (Fig. 2A-F), unlike in *T. brucei* [30,44].

We observed a higher number of MTs in the singlet region of human spermatozoa than what would be expected if only the A-tubules and CP extended to the tip (Fig. 3B–C) and, as it had previously been suggested [13], we hypothesized that dMTs could split into two complete 13-protofilament MTs. An alternative explanation for this observation could be that broken MT fragments at the flagellar tip might shift longitudinally due to the beat of the flagellum. This would lead to a higher MT count for the flagellar regions where the broken fragments are located. However, only distal MT terminations were observed in our tomograms, therefore we consider this second scenario to be unlikely. Our hypothesis that dMTs can split into two sMTs was also confirmed by the direct visualization of dMT-splitting events both in human and bovine spermatozoa (Figs 3D and 4E). Sub-tomogram averaging of the sMTs at the sperm tip confirmed that all MTs had 13 protofilaments [33]. Therefore, the formation of three additional protofilaments on the incomplete B-tubule is initiated *de novo* at the splitting locus.

In *C. elegans* neuronal sensory cilia, the cell-specific α-tubulin isoform TBA-6 together with finely-tuned post-translational polyglutamylation are required for dMT splitting and reconnection [45–47]. These same factors are likely to affect human spermatozoon ultrastructure as well, since reduced polyglutamylation caused aberrant morphologies of mice spermatozoa [52]. In addition, currently unknown structures might be involved in inducing these splitting events and in the formation of three new protofilaments. A candidate is the plus-end tracking protein EB1, since it has been reported to promote 13-protofilament MT formation [48] and tubulin sheet closure [53] *in vitro*. The small size of EB1 (30 kDa) [54,55] would further speak for this, since we saw no distinct electron densities at the site of dMT splitting. An additional hypothesis could be that a larger complex only temporarily assembles during sperm maturation to split the dMTs.

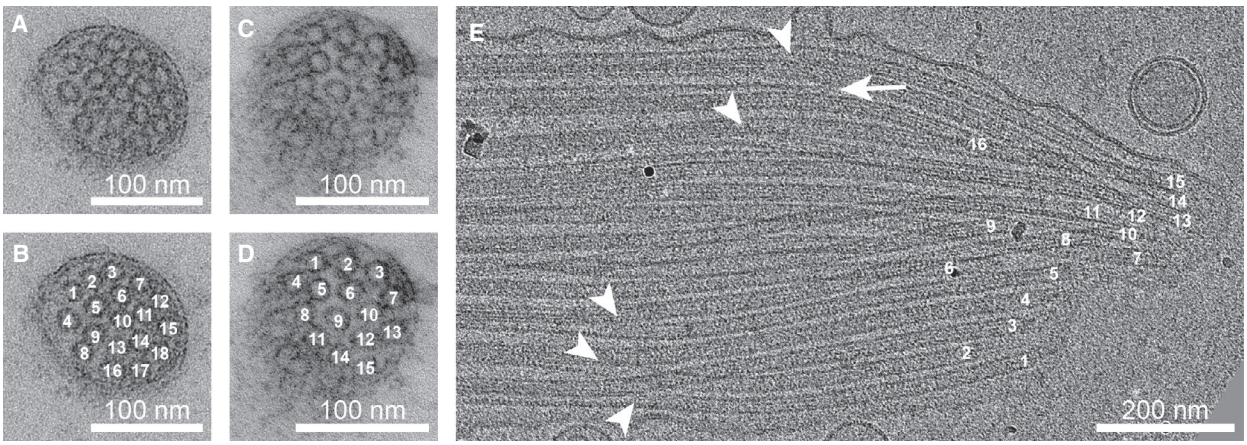

Fig. 4. Splitting of dMTs in bovine sperm flagella. Thin sections through the singlet region of bovine sperm cells show at least 18 (A–B) and 15 (C–D) sMTs. Panels A–B and C–D, respectively, show the same images, but sMTs are counted in panels B and D. (E) Cryo-EM of a flattened bovine sperm flagellum tip. Five events of dMTs splitting into two sMTs are shown (arrowheads) and at least 16 sMT ends are visible (numbered). One event of B-tubule termination is shown by the white arrow. Scale bars are 100 nm in panels A–D and 200 nm in panel E.

What advantage might the spermatozoa gain by splitting dMTs? Since the number of splitting events does not seem to be consistent between cells (in fact some do not split at all), and since the *de novo* nucleation of protofilaments in B-tubules might not be 100% efficient (Figs 3F and S3F), it is possible that they may serve as a source of variability. A high morphological intra-individual heterogeneity in human spermatozoa has been previously reported in terms of ultrastructure [37], motility and viability [56]. Given the large number of sperm cells that are produced in mammals, this may be an evolutionary strategy to ensure that some will succeed in fertilization. Another advantage of inducing sMTs might be related to the newly discovered TAILS structure, which was hypothesized to stabilize MTs in the singlet region [33]. It is possible that TAILS may stabilize sMTs more strongly than dMTs, therefore a transition from dMTs to sMTs would maximize MT stability.

The fact that more than 11 MTs exist in the human sperm singlet region has been observed previously [13,33,37]. In rodent sperm, dMTs and the CP were reported to form 'duplex' MTs that extended to the flagellar tip, where they were tied together by capping structures [32]. This suggests that splitting of dMTs may be a common phenomenon among mammals. However, contrary to rodent spermatozoa, no 'duplex' structure was observed in human flagella. MTs in the human singlet region did not terminate in pairs (Fig. 3A) and no apparent structures tied MTs together.

The CP was observed to terminate as far as 7.4 μm from the tip, in the principal piece (Fig. S1) [33]. To the best of our knowledge, no human singlet region with more than 18 MTs (which possibly originated by splitting of all nine dMTs) has been reported. Therefore, we speculate that the CP in human spermatozoa may generally terminate before any other axonemal MT, contrary to the model organism *C. reinhardtii*, where the CP extends the furthest into the flagellar tip [41,42]. This would imply that the flagellar motion, which is modulated by the CP in spermatozoa [57,58], may differ in the end piece from the rest of the flagellum. However, due to the relatively short extent of the sperm tail included in each tomogram, it was impossible to track the CP MTs through the entire end piece of every imaged cell. Therefore, we cannot exclude that some MTs observed in tomograms of singlet regions are in fact the CP. A more extensive tomography study or immuno-EM against specific CP MT markers would address this question more appropriately.

Variability in MT termination patterns was observed between different human sperm tail tips (Fig. 3A). While this could be an artifact caused by unnatural tail bending and MT sliding during the sample preparation, we find it unlikely, since the end pieces included in our analysis were not bent (Fig. S2). A similar variability in MT termination patterns was also described for rodent sperm after conventional fixation [32]. In addition, plunge-frozen *T. brucei* flagella showed comparable tip ultrastructures to high-pressure frozen or chemically fixed samples [30,44], suggesting that flagellar MT termination patterns are not noticeably disturbed during cryo-EM preparation.

We provide here the first detailed cellular 3D architecture of a human flagellar tip, revealing extensive flagellar structural variability compared to the commonly used model organisms. However, it remains to be investigated if the flagellar tip structure is conserved between different cell types in humans, for example by comparing to ciliary tips found in the upper respiratory tract. Revealing the human 3D flagellar structure will inform us of which model organism best resembles the human flagellum and should be prioritized in future ciliary research.

Acknowledgements

We thank J. Van Blerkom at Colorado Reproductive Endocrinology for providing human sperm samples from healthy patients. We thank Jonas Krantz at VikingGenetics for providing bovine sperm samples. We thank Lisa Larsson Berglund (Department of Chemistry and Molecular Biology, University of Gothenburg) for helping with high-pressure freezing of bovine sperm samples. We thank Federica Tonolo (Department of Biomedical Sciences, University of Padova) and Martin Palm (Department of Chemistry and Molecular Biology, University of Gothenburg) for helpful comments on the manuscript. JLH was supported by a Sir Henry Wellcome Postdoctoral grant and a Swedish Research Council Young Investigator Grant (number 2015-05427). EM of human samples was performed at the Boulder EM Services Core Facility in MCDB, University of Colorado, USA. EM of bovine samples was performed at the SciLifeLab national Cryo-EM facility at Umeå Core facility for EM (UCEM), Umeå University, Sweden.

Author contributions

JLH designed and supervised the study. JTC and JLH prepared samples and all authors acquired data. DZ and JLH analyzed the data. DZ and JLH wrote the

manuscript. All authors revised and approved the manuscript.

References

1 Downing KH and Sui H (2007) Structural insights into microtubule doublet interactions in axonemes. *Curr Opin Struct Biol* **17**, 253–259.
2 Gadelha C, Wickstead B and Gull K (2007) Flagellar and ciliary beating in trypanosome motility. *Cell Motil.* **64**, 629–643.
3 Nicastro D, Schwartz C, Pierson J, Gaudette R, Porter ME and McIntosh JR (2006) The molecular architecture of axonemes revealed by cryoelectron tomography. *Science* **313**, 944–948.
4 Silflow CD and Lefebvre PA (2001) Assembly and motility of eukaryotic cilia and flagella. Lessons from *Chlamydomonas reinhardtii*. *Plant Physiol* **127**, 1500–1507.
5 Witman GB (1993) *Chlamydomonas* phototaxis. *Trends Cell Biol* **3**, 403–408.
6 Hilgendorf KI, Johnson CT and Jackson PK (2016) The primary cilium as a cellular receiver: organizing ciliary GPCR signaling. *Curr Opin Cell Biol* **39**, 84–92.
7 Pazour GJ and Witman GB (2003) The vertebrate primary cilium is a sensory organelle. *Curr Opin Cell Biol* **15**, 105–110.
8 Singla V and Reiter JF (2006) The primary cilium as the cell's antenna: signaling at a sensory organelle. *Science* **313**, 629–633.
9 Bloodgood RA (2010) Sensory reception is an attribute of both primary cilia and motile cilia. *J Cell Sci* **123**, 505–509.
10 Shah AS, Ben-Shahar Y, Moninger TO, Kline JN and Welsh MJ (2009) Motile cilia of human airway epithelia are chemosensory. *Science* **325**, 1131–1134.
11 Solter KM and Gibor A (1977) Evidence for role of flagella as sensory transducers in mating of *Chlamydomonas reinhardi*. *Nature* **265**, 444–445.
12 Afzelius B (1976) A human syndrome caused by immotile cilia. *Science* **193**, 317–319.
13 Afzelius BA, Dallai R, Lanzavecchia S and Bellon PL (1995) Flagellar structure in normal human spermatozoa and in spermatozoa that lack dynein arms. *Tissue Cell* **27**, 241–247.
14 Armengot M, Milara J, Mata M, Carda C and Cortijo J (2010) Cilia motility and structure in primary and secondary ciliary dyskinesia. *Am J Rhinol Allergy* **24**, 175–180.
15 Lin J, Yin W, Smith MC, Song K, Leigh MW, Zariwala MA, Knowles MR, Ostrowski LE and Nicastro D (2014) Cryo-electron tomography reveals ciliary defects underlying human *RSPH1* primary ciliary dyskinesia. *Nat Commun* **5**, 5727.
16 Praveen K, Davis EE and Katsanis N (2015) Unique among ciliopathies: primary ciliary dyskinesia, a motile cilia disorder. *F1000Prime Rep* **7**, 36.
17 O'Toole ET, Giddings TH, McIntosh JR and Dutcher SK (2003) Three-dimensional organization of basal bodies from wild-type and δ-tubulin deletion strains of *Chlamydomonas reinhardtii*. *Mol Biol Cell* **14**, 2999–3012.
18 Sorokin S (1962) Centrioles and the formation of rudimentary cilia by fibroblasts and smooth muscle cells. *J Cell Biol* **15**, 363–377.
19 Vertii A, Hung H-F, Hehnly H and Doxsey S (2016) Human basal body basics. *Cilia* **5**, 13.
20 Vorobjev IA and Chentsov YS (1982) Centrioles in the cell cycle. I. Epithelial cells. *J Cell Biol* **93**, 938–949.
21 Kollman JM, Merdes A, Mourey L and Agard DA (2011) Microtubule nucleation by γ-tubulin complexes. *Nat Rev Mol Cell Biol* **12**, 709–721.
22 Moritz M, Braunfeld MB, Guénebaut V, Heuser J and Agard DA (2000) Structure of the γ-tubulin ring complex: a template for microtubule nucleation. *Nat Cell Biol* **2**, 365–370.
23 Zheng Y, Wong ML, Alberts B and Mitchison T (1995) Nucleation of microtubule assembly by a γ-tubulin-containing ring complex. *Nature* **378**, 578–583.
24 Szymanska K and Johnson CA (2012) The transition zone: an essential functional compartment of cilia. *Cilia* **1**, 10.
25 Afzelius B (1959) Electron microscopy of the sperm tail results obtained with a new fixative. *J Cell Biol* **5**, 269–278.
26 Carvalho-Santos Z, Azimzadeh J, Pereira-Leal JB and Bettencourt-Dias M (2011) Tracing the origins of centrioles, cilia, and flagella. *J Cell Biol* **194**, 165–175.
27 Lindemann CB and Lesich KA (2016) Functional anatomy of the mammalian sperm flagellum. *Cytoskeleton* **73**, 652–669.
28 Croft JT, Zabeo D, Subramanian R and Höög JL (2018) Composition, structure and function of the eukaryotic flagellum distal tip. *Essays Biochem* **62**, 815–828.
29 Ginger ML, Portman N and McKean PG (2008) Swimming with protists: perception, motility and flagellum assembly. *Nat Rev Microbiol* **6**, 838–850.
30 Höög JL, Lacomble S, O'Toole ET, Hoenger A, McIntosh JR and Gull K (2014) Modes of flagellar assembly in *Chlamydomonas reinhardtii* and *Trypanosoma brucei*. *eLife* **3**, e01479.
31 Fawcett DW (1975) The mammalian spermatozoon. *Dev Biol* **44**, 394–436.
32 Woolley DM and Nickels SN (1985) Microtubule termination patterns in mammalian sperm flagella. *J Ultrastruct Res* **90**, 221–234.

33 Zabeo D, Heumann JM, Schwartz CL, Suzuki-Shinjo A, Morgan G, Widlund PO and Höög JL (2018) A lumenal interrupted helix in human sperm tail microtubules. *Sci Rep* **8**, 2727.
34 Baltz JM, Oneeka Williams P and Cone RA (1990) Dense fibers protect mammalian sperm against damage. *Biol Reprod* **43**, 485–491.
35 Zhao W, Li Z, Ping P, Wang G, Yuan X and Sun F (2018) Outer dense fibers stabilize the axoneme to maintain sperm motility. *J Cell Mol Med* **22**, 1755–1768.
36 Lindemann CB (1996) Functional significance of the outer dense fibers of mammalian sperm examined by computer simulations with the geometric clutch model. *Cell Motil Cytoskeleton* **34**, 258–270.
37 Serres C, Escalier D and David G (1983) Ultrastructural morphometry of the human sperm flagellum with a stereological analysis of the lengths of the dense fibres. *Biol Cell* **49**, 153–161.
38 Eddy EM, Toshimori K and O'Brien DA (2003) Fibrous sheath of mammalian spermatozoa. *Microsc Res Tech* **61**, 103–115.
39 Kozminski KG, Johnson KA, Forscher P and Rosenbaum JL (1993) A motility in the eukaryotic flagellum unrelated to flagellar beating. *Proc Natl Acad Sci USA* **90**, 5519–5523.
40 Reynolds MJ, Phetruen T, Fisher RL, Chen K, Pentecost BT, Gomez G, Ounjai P and Sui H (2018) The developmental process of the growing motile ciliary tip region. *Sci Rep* **8**, 7977.
41 Ringo DL (1967) Flagellar motion and fine structure of the flagellar apparatus in *Chlamydomonas*. *J Cell Biol* **33**, 543–571.
42 Satish Tammana TV, Tammana D, Diener DR and Rosenbaum J (2013) Centrosomal protein CEP104 (*Chlamydomonas* FAP256) moves to the ciliary tip during ciliary assembly. *J Cell Sci* **126**, 5018–5029.
43 Gluenz E, Höög JL, Smith AE, Dawe HR, Shaw MK and Gull K (2010) Beyond 9 + 0: noncanonical axoneme structures characterize sensory cilia from protists to humans. *FASEB J*. **24**, 3117–3121.
44 Woolley D, Gadelha C and Gull K (2006) Evidence for a sliding-resistance at the tip of the trypanosome flagellum. *Cell Motil* **63**, 741–746.
45 O'Hagan R, Piasecki BP, Silva M, Phirke P, Nguyen KC, Hall DH, Swoboda P and Barr MM (2011) The Tubulin Deglutamylase CCPP-1 regulates the function and stability of sensory cilia in *C. elegans*. *Curr Biol* **21**, 1685–1694.
46 O'Hagan R, Silva M, Nguyen KCQ, Zhang W, Bellotti S, Ramadan YH, Hall DH and Barr MM (2017) Glutamylation regulates transport, specializes function, and sculpts the structure of cilia. *Curr Biol* **27**, 3430–3441.e6.
47 Silva M, Morsci N, Nguyen KCQ, Rizvi A, Rongo C, Hall DH and Barr MM (2017) Cell-specific α-tubulin isotype regulates ciliary microtubule ultrastructure, intraflagellar transport, and extracellular vesicle biology. *Curr Biol* **27**, 968–980.
48 Howes SC, Geyer EA, LaFrance B, Zhang R, Kellogg EH, Westermann S, Rice LM and Nogales E (2018) Structural and functional differences between porcine brain and budding yeast microtubules. *Cell Cycle* **17**, 278–287.
49 Moores CA, Perderiset M, Francis F, Chelly J, Houdusse A and Milligan RA (2004) Mechanism of microtubule stabilization by doublecortin. *Mol Cell* **14**, 833–839.
50 Reynolds ES (1963) The use of lead citrate at high pH as an electron-opaque stain in electron microscopy. *J Cell Biol* **17**, 208–212.
51 Kremer JR, Mastronarde DN and McIntosh JR (1996) Computer visualization of three-dimensional image data using IMOD. *J Struct Biol* **116**, 71–76.
52 Lee G-S, He Y, Dougherty EJ, Jimenez-Movilla M, Avella M, Grullon S, Sharlin DS, Guo C, Blackford JA Jr, Awasthi S *et al.* (2013) Disruption of Ttll5/stamp gene (Tubulin Tyrosine Ligase-like Protein 5/SRC-1 and TIF2-associated modulatory protein gene) in male mice causes sperm malformation and infertility. *J Biol Chem* **288**, 15167–15180.
53 Vitre B, Coquelle FM, Heichette C, Garnier C, Chrétien D and Arnal I (2008) EB1 regulates microtubule dynamics and tubulin sheet closure *in vitro*. *Nat Cell Biol* **10**, 415–421.
54 Berrueta L, Kraeft SK, Tirnauer JS, Schuyler SC, Chen LB, Hill DE, Pellman D and Bierer BE (1998) The adenomatous polyposis coli-binding protein EB1 is associated with cytoplasmic and spindle microtubules. *Proc Natl Acad Sci USA* **95**, 10596–10601.
55 Su L-K, Burrell M, Hill DE, Gyuris J, Brent R, Wiltshire R, Trent J, Vogelstein B and Kinzler KW (1995) APC binds to the novel protein EB1. *Cancer Res* **55**, 2972–2977.
56 Auger J (2000) Intra- and inter-individual variability in human sperm concentration, motility and vitality assessment during a workshop involving ten laboratories. *Hum Reprod* **15**, 2360–2368.
57 Nakano I, Kobayashi T, Yoshimura M and Shingyoji C (2003) Central-pair-linked regulation of microtubule sliding by calcium in flagellar axonemes. *J Cell Sci* **116**, 1627–1636.
58 Yoshimura M and Shingyoji C (1999) Effects of the central pair apparatus on microtubule sliding velocity in sea urchin sperm flagella. *Cell Struct Funct* **24**, 43–54.

Supporting information

Additional supporting information may be found online in the Supporting Information section at the end of the article.

Fig. S1. The number of singlet and doublet microtubules defines the singlet region.

Fig. S2. Human sperm tail tips included in the tomograms.

Fig. S3. Tomographic analysis of doublet microtubule transition modes into the singlet region.

Fig. S4. Human sperm cells with morphological deformations.

Video S1. Thickness of human sperm flagella.

Video S2. Splitting of doublet microtubules into singlets in human sperm flagella.